LAWRENCE
LIVERMORE
NATIONAL
LABORATORY

LLNL-JRNL-831192

Use of Wire Grid Polarizers with Liquid Crystal Display for Large-Volume Stereolithography

N. A. Rodriguez, H. Song, M. Chen, J. Oakdale, E. B. Duoss, C. C. Seepersad, R. H. Crawford

January 27, 2022

Additive Manufacturing

Use of Wire Grid Polarizers with Liquid Crystal Display for Large-Volume Stereolithography

Nicholas A. Rodriguez[a, b], Hongtao Song[a], Morgan Chen[a], James S. Oakdale[b], Eric B. Duoss[b], Carolyn C. Seepersad[a], and Richard H. Crawford[a]

a. Walker Department of Mechanical Engineering, The University of Texas at Austin, 204 E. Dean Keeton Street, Austin, TX 78712, United States.

b. Materials Engineering Division, Lawrence Livermore National Laboratory, 7000 East Avenue, Livermore, CA 94550, United States.

Abstract

Spatial light modulators that use liquid crystal devices (LCDs) to pattern ultraviolet light for vat polymerization suffer from a few limitations: limited range of wavelengths that can be patterned, low damage threshold for incoming light, and low efficiency of light transmission. A monochrome LCD can more efficiently transmit useful wavelengths of light for stereolithography (365-405 nm) than a color LCD, but it still contains two absorptive film polarizers that suffer from the aforementioned limitations. Wire grid polarizers reflect rather than absorb the blocked polarizations of light, resulting in a higher intensity damage threshold. They can also polarize lower wavelength light that is limited only by the wire pitch. This research investigates the effects of replacing an LCD's film polarizers with wire grid polarizers to enable polarization and patterning of high intensity UV light, resulting in shorter curing times and the ability to print a wider range of stereolithography feedstocks.

Keywords

Stereolithography, silicones, liquid crystal display, wire grid polarizer

1. Introduction

Stereolithography

Stereolithography is an additive manufacturing (AM) process that uses ultraviolet (UV) light in the form of a laser or patterned image to selectively cure a photosensitive polymer in a layer-by-layer fashion. Traditional stereolithography, as invented by Hull, uses a galvo-mirror to scan a UV laser beam across the surface of a vat of resin, curing any photopolymer that receives a high enough exposure to initiate polymerization [1]. Commercially available machines using this technique can achieve minimum feature sizes as small as 75 µm and produce a wide range of maximum part volumes as large as 1500 x 750 x 550 mm^3 [2]. However, since scanning the laser beam is a serial process, print times with this technique rapidly increase with larger build volumes and are heavily dependent on the complexity of the part geometry. Projection micro stereolithography (PµSL), on the other hand, uses a spatial light modulator, such as a digital micromirror device (DMD), liquid crystal on silicon (LCoS), or liquid crystal device (LCD), to project light over the entire build area of resin at once, rather than scanning a single point across the surface [3]. The original iterations of this technology, invented by Bertsch, Chatwin, and Monneret, all used LCDs to pattern light coming from a visible or UV laser or lamp [4] [5]. Later developments by Rosen, Wicker, Zhang, and others used digital micromirror devices (DMD) or liquid crystal on silicon (LCoS) chips to pattern the light, along with image expansion or reduction to achieve the desired image size [6] [7] [8] [9] [10].

A DMD contains an array of millions of micromirrors that each reflect the light either into either a beam dump or the desired beam path, depending on the state of each pixel [11]. An LCoS similarly patterns the light field through energizing selected pixels in a reflective liquid crystal display [12]. Using these dynamic masks allows printers to cure larger areas of resin more quickly than traditional stereolithography, as print time is not dependent on either part complexity or part footprint, and a single layer takes only as much time as required for the resin to initiate crosslinking. However, these digital masks cannot be easily scaled up in size. The chips themselves have a maximum size of around 1” diagonal, and larger images can be achieved in only two ways: magnifying the image or scanning the image across a larger area. Magnifying the image is limited by the fixed relationship between the chip size and pixel size; a larger image must also have a larger minimum feature size. DMD and LCoS chips are also limited in the maximum intensity of light that they can pattern. The DLP9500 chipset from Texas Instruments, Inc. (Dallas, TX, USA) can pattern near-UV light with a maximum intensity of 11 W/cm^2, or 26 W of total power, and this specification drops off rapidly with decreasing wavelengths [13]. This total power can create high enough intensities to initiate crosslinking over small areas, but sufficient intensities for curing less reactive silicone resins, such as the UV-curable silicones of interest in this work, cannot be achieved when the light is spread over an area exceeding a few square inches, limiting maximum part size (See Appendix A).

The other solution, if using a DMD or LCoS, is to scan the dynamically patterned image over the surface of the resin and continuously alter the image as it scans across each row to accommodate a full layer. This Large Area Projection Micro-Stereolithography technique allows larger parts to be fabricated using spatial light modulators but starts to suffer from the same downsides as traditional laser-based stereolithography. This approach requires longer layer times that are dependent on the part’s footprint and may result in distorted features as the image is scanned across more extreme distances [14].

A third vat polymerization technique, masked stereolithography (MSLA), uses a liquid crystal device (LCD) screen with a near-UV backlight to produce a patterned image on the resin surface [15]. This light patterning source also typically comes from below the resin bath and can use either a color or monochrome LCD screen. Color LCDs contain a color filter which consists of three sub-pixels, each passing only red, green, or blue light. Only the blue color filter will transmit any light near the UV spectrum, so these screens are limited in their usefulness for curing some photopolymers and must be used with resins that are reactive to visible wavelengths of light [16]. Figure 1 depicts light traveling through the patterning components in a masked SLA system, which include two polarizers oriented orthogonally to one another with an LCD screen between them.

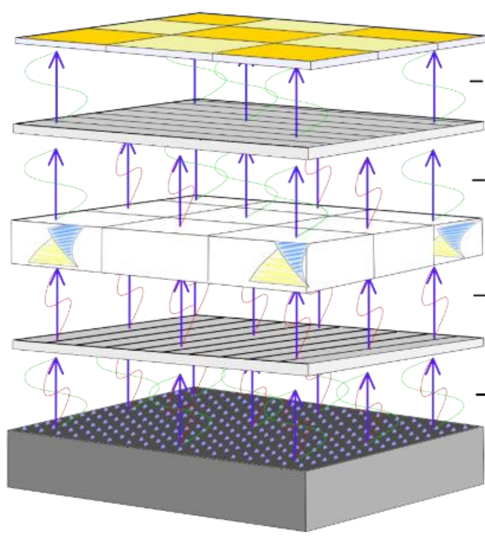

Figure 1: Diagram of unpolarized light through components in stereolithography printer

Previous efforts at 3D printing with masked SLA have used both color and monochrome LCD screens, but both techniques are limited to printing with visible wavelengths of light at low intensities of around 1 mW/cm^2. Fei used a color LCD with film polarizers to pattern 405 nm light to cure silica slurries. [17] [18]. The photopolymer component of the slurry was acrylatedbased, specifically hexane diol diacrylate (HDDA), combined with a hydroxy-ketone photoinitiator, which is a combination that has been shown to cure readily at low intensities even with visible wavelength light [19] . Wu studied decreased separation forces while curing resin and used a color LCD screen to pattern 405 nm light with an intensity at the build plane of 1.49 mW/cm^2 [20]. This same printer was used to cure ceramic slurries with an intensity of 1.4 mW/cm^2 [21]. Wang used an LCD printer (Currax Solutions Inc., Kelowna, BD, Canada) to cure an acrylate-based resin (Spot-LV, Spot-A Materials, Barcelona, Spain) [22]. The intensity is not reported, but this resin has been cured elsewhere with 405nm light at intensities below 1 mW/cm^2 [23].

One of the goals of this research is to enable printing with a larger variety of resins, including photocurable silicone elastomers. Silicones display many desirable properties including high thermal and thermo-oxidative stability, stability towards UV-radiation and general chemical inertness [24]. One of the more remarkable attributes of silicone rubbers is their wide service window, ranging from -100 ^oC to >250 ^oC. In our previous work, we designed an actinic silica/resin reinforced silicone formulation and demonstrated its 3D-printability using a DMD-SLA approach [25]. One of the ultimate goals of this research is to develop a tunable silicone formulation that can be adapted on the fly to meet varying mechanical requirements (i.e. extensibility, hardness, modulus) while still preserving excellent toughness and minimal compression set. Initial forays into UV-curable silicones utilized radical-mediated thiol-ene crosslinking for the curing chemistry, but lack of available commercial materials and observed poor mechanical aging at high temperatures led towards UV-initiated platinum-catalyzed hydrosilylation, instead. Pt-catalyzed hydrosilylation is a common and well-known strategy for RTV-silicone formulations, and several UV-activated platinum catalysts have been developed

[26]. However, examples of photocurable silicones based on UV-activated platinum catalyzed hydrosilylation have required high light intensities to reach gelation. Early examples by Oxman and Boardman described irradiating samples with a high-pressure mercury-vapor lamp filtered to illuminate the resin with an intensity of 525 mW/cm^2 at wavelengths ranging from 390-485 nm, with the resin reaching its gel point after 48 seconds [27]. A more recent example by Obata et al. utilized a 355 nm laser that exposed the sample with a similar fluence of 21,220 mJ/cm^2 [28].

These prior efforts at developing photocurable silicones based on platinum catalyzed hydrosilylation, or PCHS-silicones, indicate the necessity of high-intensity and low-wavelength UV light in order to minimize the curing time for each 3D printed layer. This need is exacerbated when attempting to cure this resin over a large area of greater than a few inches. All of the currently available light patterning techniques fail in their capability to deliver high intensity (>100 mW/cm^2) UV light over large areas. This indicates a need to develop a new light patterning technique, described here as masked, or LCD, stereolithography with the film polarizers replaced with wire grid polarizers.

Polarization

Monochrome LCDs, as opposed to color LCDs, do not have color filters and are much more efficient at patterning lower wavelength light. Accordingly, they can be used with near-UV and UV light sources. Apart from the color filters, the two linear film polarizers are the components in an LCD screen that absorb the largest percentage of incoming light. An LCD screen's backlight provides unpolarized light whose electric field oscillates perpendicularly to the direction of propagation but fluctuates randomly in time. Each polarizer transmits light with an electric field oscillating in a single plane and blocks light that oscillates orthogonally to that plane. Therefore, an inactive LCD screen with two polarizers oriented orthogonally to one another will block all incoming light, while an active LCD screen's energized pixels will rotate the polarization of light passing through each pixel, allowing it to be transmitted through the second polarizer. Ideal polarizers behave according to Malus' law, by which the intensity of light transmitted through a polarizer is computed as:

$$I=I_0*\cos^2(\theta), \tag{1}$$

where θ is the angle between the incident electrical field and the axis of transmission for the polarizer. Since any portion of unpolarized light's electric field can be composed of a component that is parallel to the direction of ray propagation and perpendicular to it, p- and s-polarized light, respectively, unpolarized light can be assumed to have an equal distribution of the two orthogonal polarizations. Therefore, when light impinges on an ideal polarizer, one-half of its intensity is expected to be transmitted. In reality, due to surface reflections entering and leaving the polarizer and parasitic absorption, less than 50% of the light is transmitted, and the efficiency of this transmittance changes for different types of polarizers. Film polarizers transmit approximately 25% of incoming light, whereas wire grid polarizers can transmit up to 44% of incoming light at 405 nm [29] [30]. The difference between ideal and actual transmission for the two types of polarizers is related to the amount of light that is absorbed by the polarizer, which is defined by the material's absorption coefficient.

In addition to the difference in transmittance efficiency for film and wire grid polarizers, they also have different mechanisms for polarizing light. The film polarizers used in LCD screens are made of stretched sheets of polyvinyl alcohol (PVA) and are absorptive polarizers; they transmit polarizations of light that are parallel to the stretched PVA chains and absorb all others. These polarizers have three main disadvantages for use in stereolithography (1) they do not transmit significant amounts of UV light; (2) they are inefficient at transmitting light at all wavelengths; and (3) they absorb light that is not transmitted, resulting in a relatively low maximum intensity of light before overheating. A different method of polarizing light is a wire grid polarizer, which consists of nano-scale metal wires deposited on a substrate in parallel lines with a pitch less than one third of the wavelength of light to be polarized. These wires reflect any light with a component of its electrical field aligned with the wires and transmit the rest of the light with an electrical field perpendicular to the wires. Therefore, similarly to film polarizers, the use of two wire grid polarizers oriented orthogonally to one another reflects all light and appears to be a mirror. Since the wavelength of light to be polarized must be greater than the pitch of the metal wires, wire grid polarizers are most commonly used to polarize higher wavelengths of light, such as microwaves and infrared [30]. While the laser induced damage threshold for a film polarizer is only 1000 mW/cm^2, wire grid polarizers can withstand much higher intensities since they reflect, rather than absorb, the majority of light that is not transmitted [29]. These intensities are only limited by the maximum temperatures of the constituent materials, such as fused silica and aluminum.

No attempts at using LCDs for stereolithography have incorporated wire grid polarizers in place of their original film polarizers, and therefore, these approaches have been limited to curing resins that are highly reactive to visible light at relatively low intensities of under 10 mW/cm^2 [17] [20] [22]. Research into curing less reactive resins that need higher intensities and lower wavelengths of light has been limited by at least two factors. First, large, high-resolution

(4K or 10MP) monochrome LCD screens are not widely available and are much more expensive than comparable color LCDs. Second, wire grid polarizers are more difficult to manufacture as the wavelength of light decreases because the wire pitch must be smaller than one-third the wavelength of light. Also, scaling these polarizers up to large areas increases cost significantly. For curing traditional SLA resins, replacing an LCD's polarizers with wire grid polarizers is not necessary, as sufficient intensities of light can be transmitted by a monochrome, or even a color, LCD screen with its original film polarizers. However, these techniques cannot be used to print with resins that require intensities of light exceeding 50 mW/cm^2, such as PCHS-silicones. Although the use of large wire grid polarizers and monochrome LCD screens has not been previously explored due to their high costs, use of these components appears to be the most feasible light patterning technique to cure PCHS-silicones on a large scale.

This paper details the creation of a COMSOL model and a series of physical experiments to characterize the optical and thermal performance of the proposed light patterning technique, which consists of wire grid polarizers coupled with an LCD screen, compared to a typical LCD screen with film polarizers. Section 2 describes the experimental methods for characterizing light transmittance and contrast of the two light patterning techniques and summarizes the COMSOL simulation conditions for predicting optical and thermal performance. Section 2 also details the resin formulations and curing conditions for this research. Section 3 provides details on a new boundary condition developed in COMSOL's Ray Optics module that enables the modeling of a reflective, nonideal polarizer. Section 4 compares the experimental optical performance of the two light patterning techniques to determine the preferred technique for curing PCHS-silicones. Section 4 also presents a variety of 2D patterns cured using the LCD with wire grid polarizers. Finally, Section 4 validates the COMSOL model's predicted thermal behavior of the wire grid polarizer and LCD under high-intensity illumination, experimentally determines a maximum temperature for the LCD before failure, and presents new illumination strategies to reduce the maximum temperature of the LCD during long periods of curing.

2. Experimental Materials and Methods

2. 1. Light Patterning Characterization

A series of tests was conducted to understand how light at decreasing wavelengths transmits through color and monochrome LCDs using both film and wire grid polarizers. The test bed consisted of LED arrays at 365, 385, 405, and 450 nm from the same manufacturer (Violumas, Fremont, CA), with each capable of outputting light up to 1000 mW/cm^2; a photometer with two probes that measures light at all four wavelengths with an appropriate conversion factor; a Blackeye USB 3 camera (FLIR, Wilsonville, OR) with a 25 mm lens; and a three-axis motion stage to translate the probe and camera to explore the spatial profile of the light field. A UV2600 spectrometer (Shimadzu, Kyoto, Japan) was used to validate the transmittance testing and gather data on the wire grid polarizer's reflectance over the relevant wavelength range. Temperature measurements for the LCD screens and both types of polarizers were gathered with K-type surface mount thermocouples. Figure 2 shows the testbed used to collect light transmittance data.

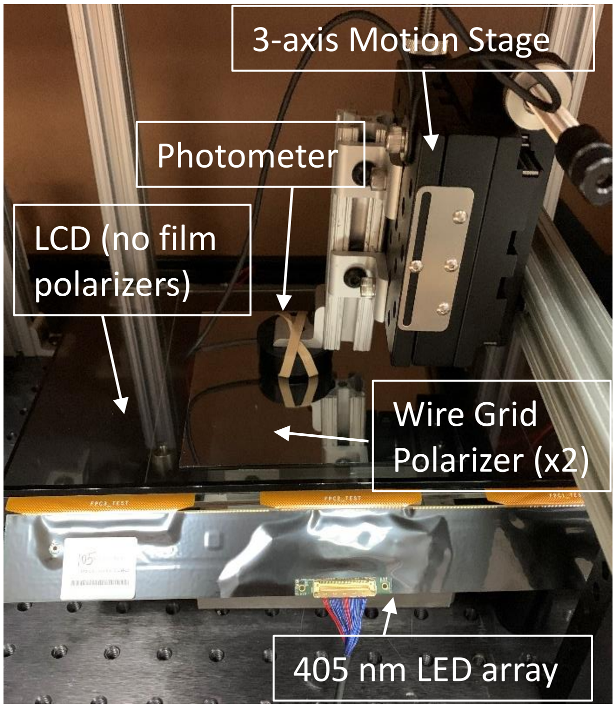

Figure 2: LED array and light patterning components

Transmittance tests were conducted on color and monochrome LCDs containing both PVA film (Thorlabs) and wire grid (NILT) polarizers. The wire grid polarizers have a pitch of 50 nm and consist of aluminum wires on a fused silica substrate. The two LCDs (DuoBond, Guangdong, China), one color and one monochrome, have 13.3" screens with a pixel resolution of 3840 x 2160 and pixel pitch of 76.5 µm. The transmittance efficiency of the two types of polarizers was measured by placing the photometer probe at a fixed distance of 50 mm from the LED array and taking an initial baseline measurement without polarizers followed by another measurement with a single polarizer in the optical path prior to the photometer probe. These tests were then repeated using each of the LCD screens with their original film polarizers first intact and then replaced with wire grid polarizers. For transmittance tests that included the LCD screen, the screen was set up as a second monitor that displayed a fully white image. Transmittance testing was conducted at intensities ranging from 100 – 1000 mW/cm^2. Temperature measurements of the polarizers and LCDs were taken using a K-type surface mount thermocouple adhered with thermal paste to the distal surface of each component relative to the light source. These thermal tests were conducted using 385 and 405 nm light at higher intensities ranging from 1000-2000 mW/cm^2 measured proximal to the component's surface for cycles of up to 120s of illumination followed by either passive or forced air cooling with a 35 mm fan blowing over the component's surface.

The contrast and expected minimum feature resolution for the light patterning system was determined by calculating the Modulation Transfer Function (MTF), which is defined as follows:

$$MTF = \frac{I_{max} - I_{min}}{I_{max} + I_{min}} \tag{2}$$

where I_{max} and I_{min} represent the maximum and minimum intensities achieved by alternating black and white line pairs, respectively. The system's ideal contrast can be determined by measuring the light intensity through a fully white screen compared to a fully black screen. The minimum resolvable feature size of the light patterning system can be determined by observing how this ideal contrast decreases for patterning a series of black and white line pairs with increasing spatial frequencies and calculating the MTF for each frequency according to Equation 2.

MTFs that approach 1.0 are achieved when there is a large difference in intensity between the white and black lines; in contrast, white and black lines that are closer to grey will have a decreased contrast represented by an MTF approaching zero. The spatial frequency of line pairs for which the MTF is 0.5 can be considered the smallest resolvable feature size [31].

To conduct these tests, the camera's filter was removed from its placement in front of the sensor, since it filtered out UV light increasingly at lower wavelengths. The camera was then placed at varying distances from the LED array to determine the homogeneity of light. After the light field's intensity was validated to be homogeneous over the illuminated area, the achievable contrast for two light patterning techniques at the four wavelengths was calculated. The light patterning components – a monochrome LCD with both its original film polarizers, one film replaced with a 50nm half-pitch wire grid polarizer, and both films replaced with wire grid polarizers – were positioned so that the distal surface of the second polarizer was 50mm away from the LED array at the previously determined plane of homogeneous light.

The line pair images were created in MATLAB (MathWorks, Natick, MA) with line pairs ranging from one to five pixels per line over a 3840 x 2160 pixel area corresponding to the size of the 13.3" monochrome LCD screen. The patterned line pairs were imaged by the CCD, which was paired with a 25 mm focal length lens at a working distance of 150 mm. The images were processed using MATLAB's `imread` function, and the intensity of light was extracted for each pixel encompassing a line orthogonal to the line pairs. Peak and valley intensities along the line were averaged to calculate the MTF.

2. 2. Resin preparation and curing

The illumination and light patterning systems' minimum curable feature size was tested on the UV-curable resin PR48 (Colorado Photopolymer Solutions, Boulder, CO) by projecting line pairs with decreasing spatial frequency and observing the lowest spatial frequency that could be resolved. This resin was chosen as it has well-understood curing parameters and behavior, and it allows us to characterize the resolution of the light patterning system. In addition to PR48, a photocurable silicone was developed based on a platinum catalyzed hydrosilylation reaction that is reactive under UV illumination. The resin consisted of vinyl-terminated PDMS, DMS-V33, and hydride-terminated PDMS, HMS-H271, (Gelest, Morrisville, PA) with respective concentrations to achieve a molar ratio of vinyl to silane of 1:1.7. A Thinky (Laguna Hills, CA) ARV-310 vacuum mixer was used to mix 100 ppm (Trimethyl)pentamethylcyclopentadienylplatinum(IV) (Strem Chemicals, Newburyport, MA), 300 ppm 9, 10-Dibutoxyanthracene (BOC Sciences, Shirley, NY), 200 ppm 2,5-bis(5-tert-butyl-benzoxazol-2-yl)thiophene (99%) (Sigma Aldrich, St. Louis, MO), and 60 ppm 1-ethynyl-1-cyclohexanol.

Curing of the two resins, PR48 and photocurable silicone, was conducted with a 405 nm LED array with an intensity of 15 mW/cm^2 and a 385 nm LED array with an intensity of 85 mW/cm^2, respectively, where the intensity was measured after the light patterning components. Test samples of PR48 and PCHS-silicone were exposed to the light for 1s and 20s, respectively, followed by a resting period of 30s before the uncured resin was cleaned from the samples using ethanol or Dynasolve M10 (Ellsworth Adhesives) for the PR48 and silicone resins.

3. Simulations

Modeling Optical and Thermal Behavior of Illumination and Light Patterning

The illumination and light patterning system was simulated in COMSOL via a two-step process using the Ray Optics module combined with heat transfer modeling. COMSOL’s Ray Optics module is a ray tracing program intended to model light on geometric scales far larger than the light’s wavelength. It can simulate each ray’s intensity and polarization through Stokes parameters and includes built-in boundary conditions to model polarizers, wave retarders, and diffraction gratings, among other optical devices. This module was used to model a 400 mm x 400 mm LED array and light patterning components consisting of two reflective wire grid polarizers on either side of an LCD screen, as depicted in Figure 3. These components were used in the experimental sections of this research and are designed for implementation in the large-volume, high-viscosity stereolithography printer that is the ultimate goal of this research.

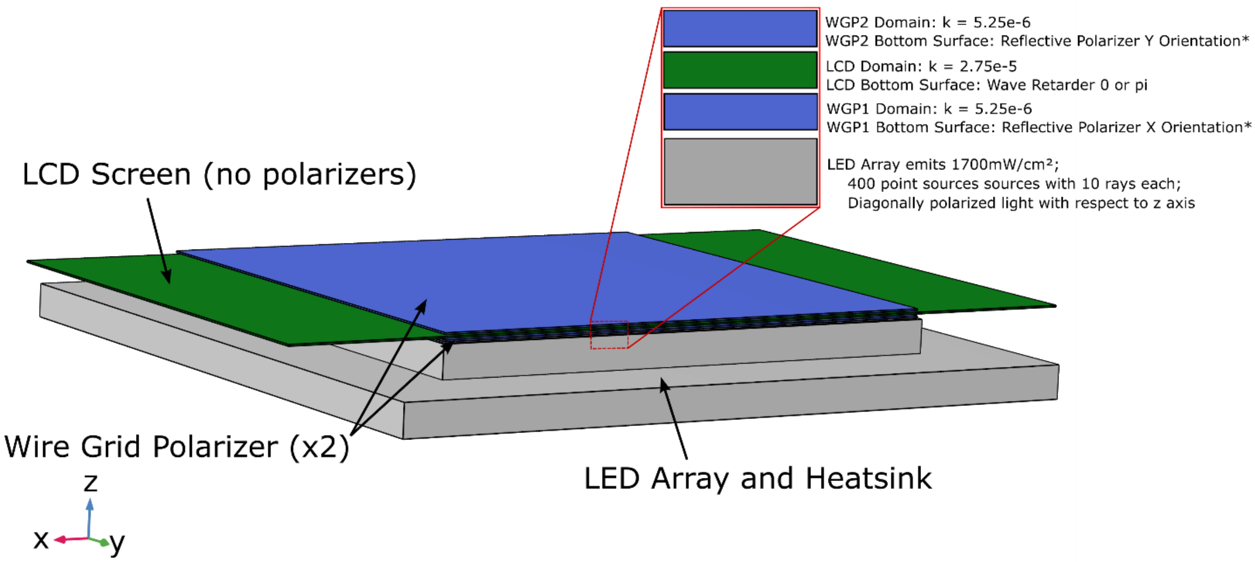

Figure 3: Components and boundary conditions for modeling light patterning and thermal behavior of stereolithography components

The conditions for the COMSOL model were derived from prior experiments that were conducted in developing the photocurable PCHS-silicone. From these experiments, the photocurable silicone was found to cure optimally under 385 nm illumination with an intensity of 85 mW/cm^2 and a curing schedule consisting of 20 seconds of illumination followed by at least 20 seconds of dark cure time. Based on an expected 5% transmittance of the light from its source to the build plane, the LED array was given a starting intensity of 1700 mW/cm^2, or a total power of 2.72 kW spread over 1600 point sources, with each emitting a cone angle of 15°. Ten rays were traced from each of the point sources over 0.8 ns, a sufficient time for the rays to pass through the patterning components and for the rays initially reflected off the first polarizer to make a second pass through the patterning components. The light sources were initialized with a diagonal polarization, so they had equal components of x and y polarizations, similar to unpolarized light.

The light patterning system consists of two reflective polarizers and an LCD screen. In COMSOL's Ray Optics Module, the LCD screen's pixels can be modeled as a series of wave retarders with retardance of either 0 or π, depending on the state of each cell. COMSOL also has a linear polarizer boundary condition, polarizes incoming light rays when applied to a surface; however, this condition cannot accurately model the behavior of non-ideal or reflective polarizers. The boundary condition simply rotates the polarization of light to align with a preset transmission axis and decreases each ray's intensity by a constant proportion depending on the incoming light's polarization. It does not inherently generate reflected rays and cannot be modified to do so; therefore, further methods of modeling reflective polarizers must be explored.

To simulate a wire grid polarizer, two main functionalities of the polarizer need to be modeled. First, the polarizer should reflect and transmit portions of each ray's intensity as a function of the ray's polarization compared to the polarizer's transmission axis. Second, the polarizer should rotate each ray's polarization ellipse about the direction of propagation to be aligned with the transmission axis. Similarly, the reflected ray's polarization should be rotated to have a polarization orthogonal to the transmission axis. In addition to these two functions, the non-ideal representation of the polarizer should also absorb a portion of light that is neither reflected nor transmitted and serves as a heat source in the thermal model.

The polarizer's domain was assigned a diffraction grating boundary condition that inherently transmits refracted rays and creates new reflected rays. In contrast, the linear polarizer boundary condition can only transmit rays and cannot generate new reflected rays. Wire grid polarizers have previously been modeled as zero order diffraction gratings [32]; however, in this simulation, the diffraction grating condition is used only as the framework through which a wire grid polarizer can be modeled. Figure 3 shows the boundary and domain conditions used to model light propagating through the two wire grid polarizers and LCD screen.

The formulas defining light rays leaving the diffraction grating are defined in COMSOL's equation editor. A light ray's polarization ellipse is defined inherently by COMSOL using a global coordinate system, but this definition introduces errors in the calculations for rays that are not traveling orthogonal to the polarizer. Therefore, new variables were created to define each light ray's x and y polarization, or the polarization components orthogonal to the ray propagation (See Figure 1) on a local coordinate system with respect to the ray's direction of propagation. The ratio of these local x and y polarization components can be used for two functions. First, the ratio of x-to-y polarizations can be used in conjunction with the polarizer's transmission axis to determine the percentages of light that should be transmitted and reflected. Second, the ratio of the x-to-y polarization components can also be used to calculate the angle by which each ray's polarization ellipse must be rotated to align it with the polarizer's transmission axis. A detailed discussion of these modifications can be found in Appendix B, and a validation of the polarizer's two main functions can be found in Figure 4.

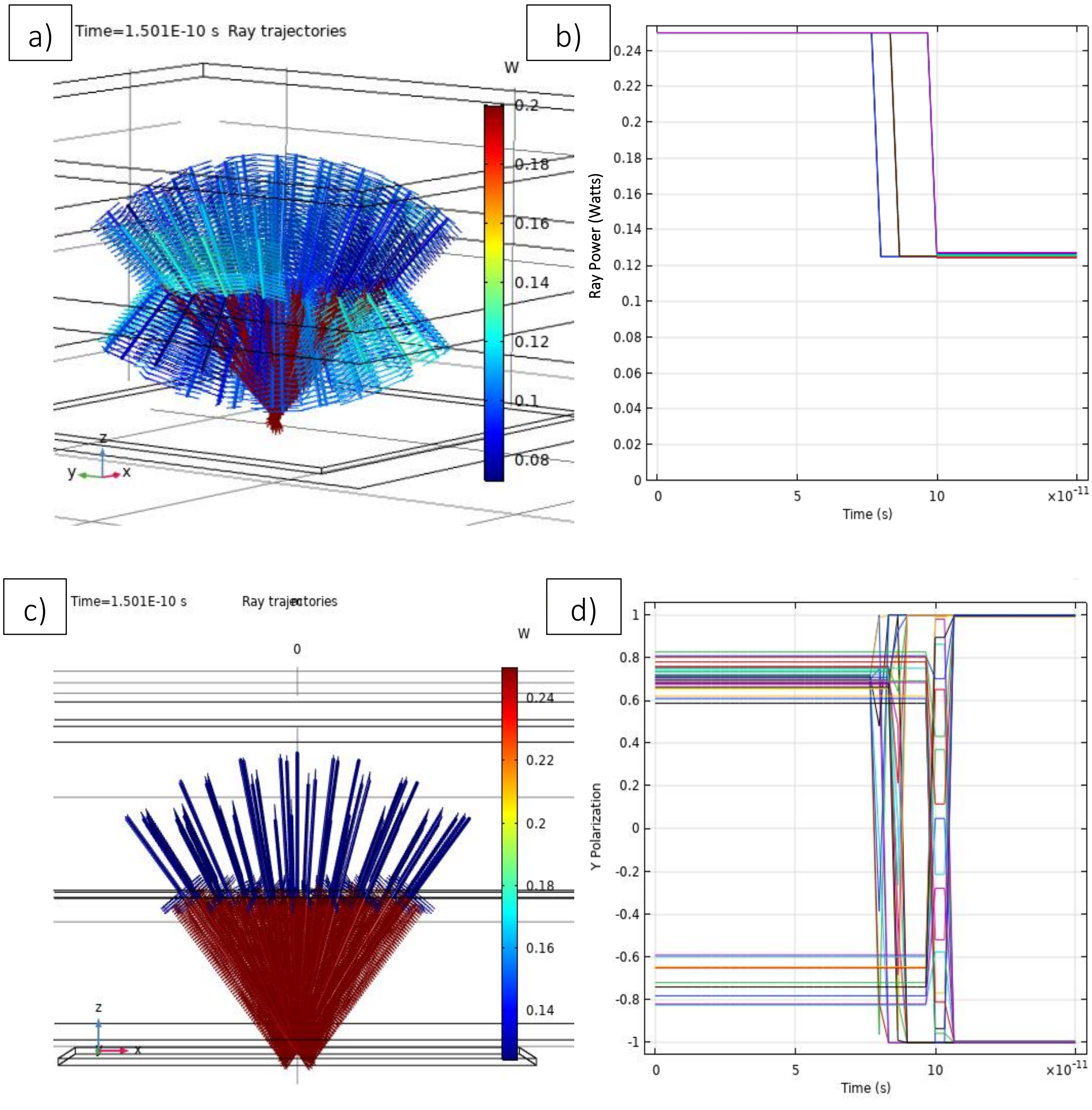

Figure 4: Validation of reflective polarizer functionalities a-b) 50% of each ray's power is reflected at polarizer surface; c-d) transmitted rays' polarization ellipse is aligned with polarizer tranmission axis (y-axis)

Figure 4a and 4b illustrate the polarizer function of reflecting and transmitting proper proportions of the incoming light based on its polarization. The example light source has a diagonal polarization, so 50% of the light should be transmitted and 50% reflected, and that performance is confirmed in the plot of Figure 4b. This figure plots the power of a few selected rays which each drop by half as they pass through the polarizer. Rays at a larger cone angle reach the polarizer slightly later in time. Figure 4c and 4d depict the second polarizer function, which is to rotate the polarization of light to be aligned with the polarizer's transmission axis. In this example, the transmission axis is the y axis, or in and out of the page, and each ray's polarization is represented by a series of orthogonal lines along its direction of propagation. The ray polarizations are diagonal in the red section before the polarizer and are rotated to be parallel to the y axis after the polarizer. Figure 4d plots the y component of the polarization ellipse, which is rotated from $\pm\sqrt{2}/2$ (diagonal) to ± 1 (aligned with y axis) after passing through the polarizer.

Modeling how light propagates through the patterning system in a real scenario also involves assessing how light is absorbed by each domain. This absorption in COMSOL is determined based on each domain's imaginary refractive index, a wavelength-dependent material property related to the absorption coefficient. As light propagates through a domain, its intensity is attenuated based on the imaginary refractive index. This absorbed light is converted into a heat source, which is used as an input variable for the second step of the simulation: heat transfer modeling. The imaginary refractive indices of the WGP and LCD for this simulation were 5.25×10^{-6} and 2.75×10^{-5}, respectively. The imaginary refractive index, k, for the WGP was determined experimentally from spectroscopy results shown in Figure 5. For 385 nm light, the WGP transmits 41% and reflects 43% of light, leaving 16% that is absorbed. For the LCD, k was extrapolated from BK7 glass (k = 1.7e-8), ITO film (k = 0.05), and PCH-32 liquid crystal (k = 3e-7) with thicknesses of 1.25 mm, 700 nm, and 5 µm, respectively [33] [34] [35].

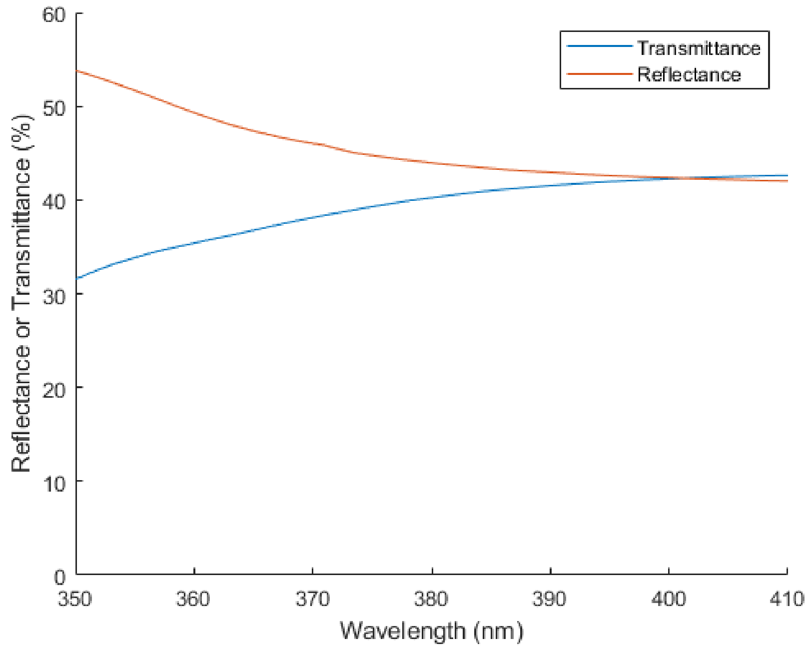

Figure 5: Reflectance and transmittance results from spectroscopy on a 50 nm half-pitch wire grid polarizer

Following the nanosecond-scale ray tracing step, these imaginary refractive index values were used to define how light is absorbed through the light patterning components in order to conduct a heat transfer simulation with the absorbed light as heat sources. These heat sources were applied for varying times up to 20 seconds and then removed for cooling periods before repeating the heating cycle. Conduction and radiation were modeled using material properties for the polarizer and LCD's bulk materials, which are fused silica and borosilicate glass, respectively, and each were given an emissivity of 0.9. Natural convection boundary conditions were applied to each surface of the light patterning components, and the heat transfer coefficient was calculated by COMSOL from the orientation of each surface as well as the geometry and material of each component, with air having a relative humidity of 0.6. The air temperature was set at room temperature for surfaces of the wire grid polarizers and LCD that are not bounded immediately by another component but are open to ambient air. In contrast, for portions of the

LCD and WGP surfaces that only have a small (2.5 mm) air gap between themselves and the surface of another light patterning component, air temperature was averaged between room temperature and the surface temperature of the opposing component. Forced convection was modeled similarly for select cases with an air speed of 2.5 m/s.

In addition to these thermal modeling conditions, the two-step simulation used for this research incorporates the previously discussed modifications to COMSOL's definition of a polarizer that successfully rotate the polarization of light, reflect any light with a polarization not aligned with the transmission axis, and absorb the correct proportion of transmitted light to convert it into a heat source. This new boundary condition for a nonideal reflective polarizer is applied to both of the wire grid polarizers that constitute a portion of the stereolithography printer's light patterning system. With this model of the light patterning components, the COMSOL model can be used to predict the temperature of the polarizers and LCD screen during high-intensity UV illumination and subsequent cooling.

4. Results and Discussion

4. 1. Predicting and Minimizing the Temperature of Light Patterning Components

Since the wire grid polarizers and LCD screen heat up rapidly during illumination, it is important to monitor and predict the temperature of the light patterning components under illumination. Using the boundary conditions described in Section 3 for reflective, non-ideal wire grid polarizers, the COMSOL model was used to predict both optical and thermal behavior of the components of a 400 mm x 400 mm light patterning system. Experimental results are used to validate the thermal behavior of the model so that it can be used to investigate techniques to reduce the components' maximum temperatures. Figure 6 shows an example of thermal results from the COMSOL simulation as well as the experimental test bed used to validate that model.

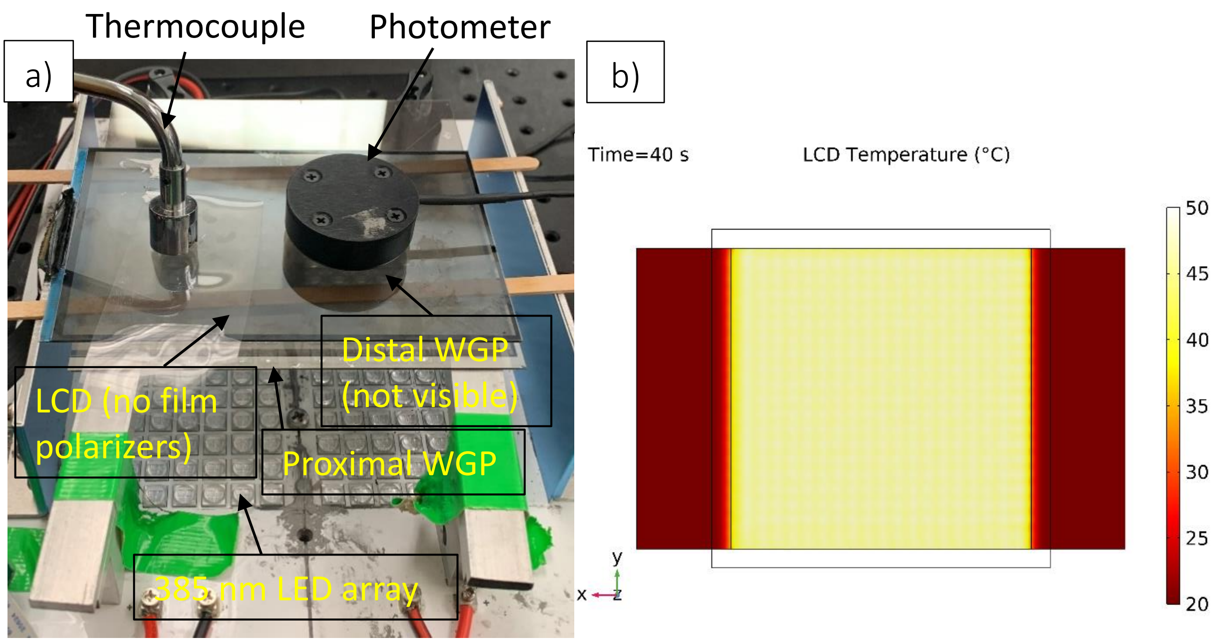

Figure 6: a) Experimental 6" x 6" LED array and light patterning components b) Temperature of LCD distal surface after 20s illumination and 20s cooling with forced convection

To validate the predicted thermal behavior of the light patterning components, temperature measurements were taken on the distal surface of the proximal wire grid polarizer during a 20s illumination of 385 nm light with an intensity of 1700 mW/cm^2. A subsequent experiment with identical illumination conditions recorded the temperature of the distal surface of the LCD screen, and both experiments were conducted without forced convection. The maximum temperatures reached by the polarizer and LCD were 50°C and 89°C, respectively, and the temperatures were also recorded during cooldown periods after illumination. The same illumination conditions were simulated in COMSOL using two wire grid polarizers that were modeled according to the discussion in Section 3 and an LCD screen with cells modeled as a wave retarder with retardance of π or 0. For both the thermal experiment and simulation, the LCD was fully white with the liquid crystal fully rotating the polarization of light across its entire surface. The maximum surface temperatures of the proximal wire grid polarizer and LCD from the COMSOL simulation were plotted along with the experimental temperature data for the same components in Figure 7.

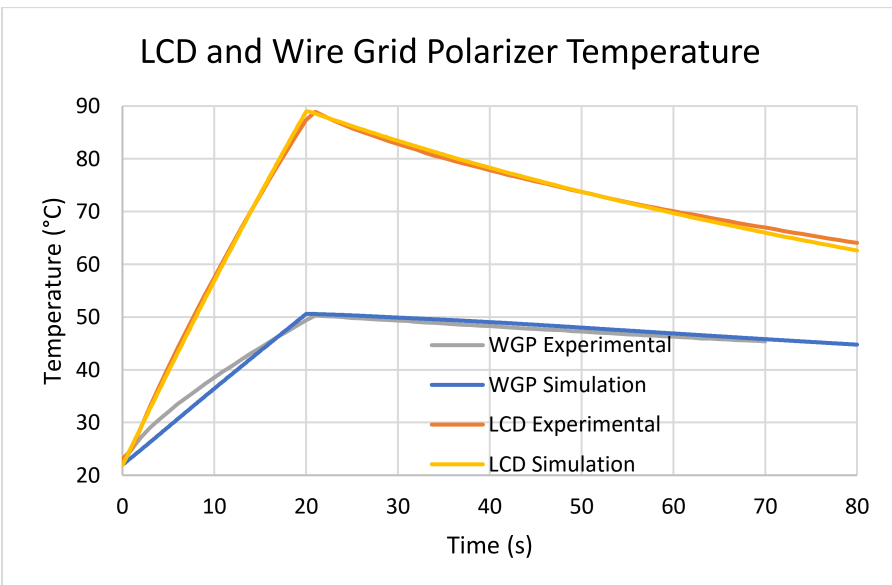

Figure 7: Measured and predicted temperatures of a) WGP and b) LCD under high-intensity illumination

For the wire grid polarizer, the predicted rate of heating is slightly more linear than the experimental data, suggesting the simulation is not fully modeling some nonlinear thermal behavior and might have both higher heating and cooling rates. However, the maximum predicted temperature and subsequent cooling when the light source is turned off both match the experimental values well. After 20s of illumination, the polarizer heats to 50°C, and the largest error between real and predicted temperatures is 2.9°C, which occurs at 5s. However, the more critical component to monitor is the LCD screen, which heats to 89°C after 20s of illumination, and the error between this observed temperature and the predicted maximum temperature is less than 1°C. The predicted minimum temperature of the LCD after a one-minute cooling period is 62.6°C, which is 1.4°C cooler than the experimental temperature at that time.

To determine the maximum temperature of the LCD before failure, the LCD was subjected to increasing durations of light exposure at an intensity of 1700 mW/cm^2, and its ability to pattern light was verified by measuring the intensity of light being transmitted through a white screen. Light transmittance can be used to determine the temperature at which the LCD fails, since the liquid crystal becomes less efficient at rotating the polarization of light, and eventually fails to rotate the light at all when it reaches higher temperatures. Experimental LCD temperature and transmitted intensity are plotted in Figure 8.

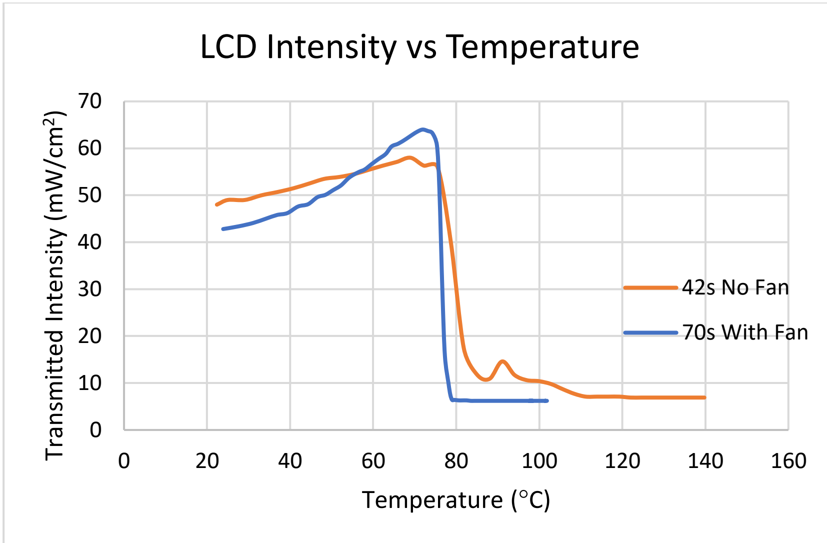

Figure 8: Experimental LCD transmitted intensity as a function of LCD temperature under high-intensity illumination

The data in Figure 8 shows temperature for two experiments under identical illumination conditions, with the only difference being the application of a fan for forced air convection. Although the screen heats at different rates, in both experiments the transmitted intensity drops off rapidly after the screen reaches a temperature of 75°C, which is considered the maximum allowable temperature for this system.

For most commercially available resins, this light patterning system would be illuminated for only a few seconds at a time to initiate curing, and heating of the components would not be significant. However, for curing the PCHS-silicone, high-intensity illuminations for up to 20s could be required. To ensure the LCD remains at low enough temperatures during curing of the silicones, experiments were conducted to explore varying convection and illumination conditions while monitoring the LCD's temperature at its distal surface to the LED array. Forced air convection was implemented with an air velocity of 2.5 m/s and room temperature air (20°C). Additionally, staggered illumination sequences were explored by alternating active curing (illumination) and passive curing (dark periods) while maintaining the 20s of illuminated and 20s of non-illuminated curing times required by the silicone. Figure 9a lists the LCD's maximum experimental temperatures under the various illumination and convection conditions, and Figure 9b plots both experimental and simulation LCD temperatures.

Maximum Experimental LCD Temperature (°C)		
Illumination Sequence	Fan On	Fan Off
20s	71.0	88.9
10/10s	64.7	85.3
5/5/5/5s	61.3	83.9

b)

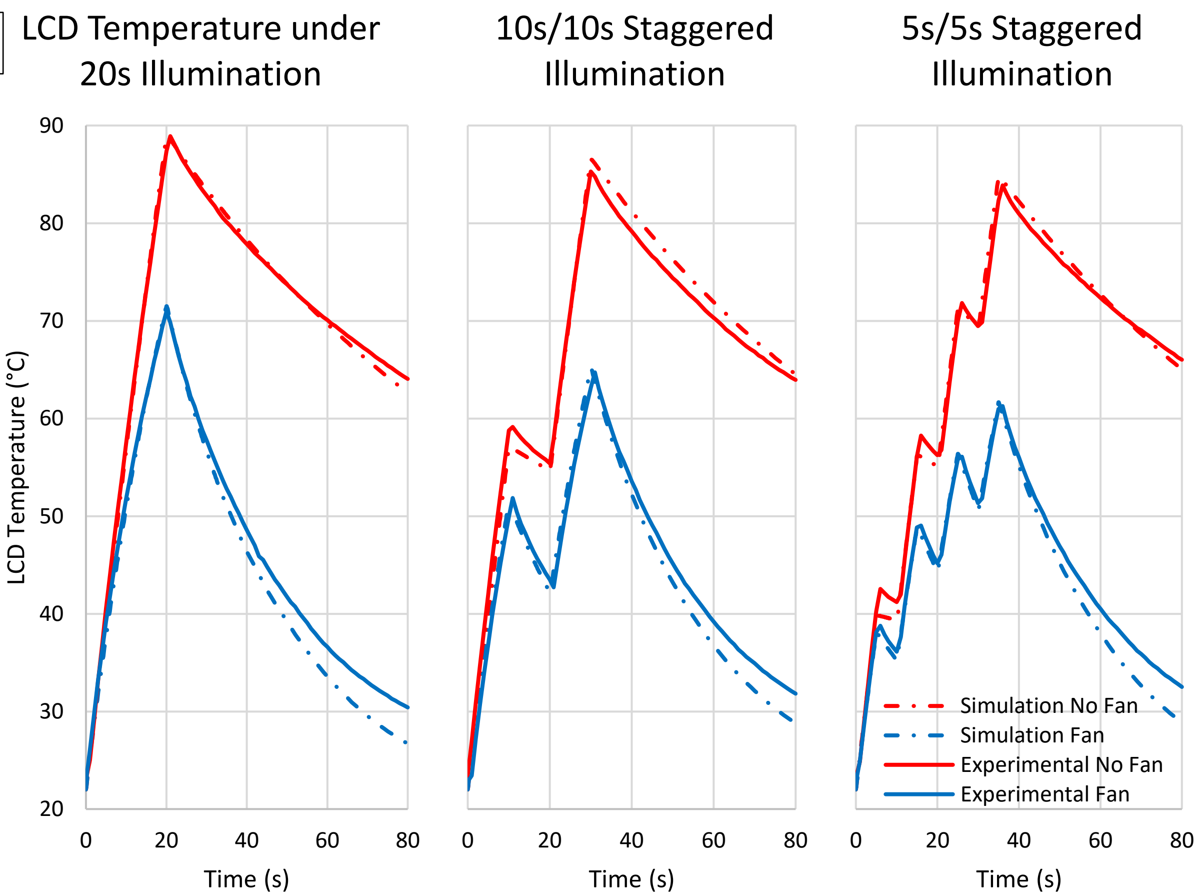

Figure 9: a) Maximum experimental temperatures reached by the LCD under the varying illumination and convection conditions, b) LCD temperature during staggered illumination sequences with and without forced convection

The maximum temperature reached by the LCD during an experimental 20s illumination is decreased by 17.9°C with the application of a fan and is decreased by an additional 9.7°C with the implementation of staggered illumination in 5s phases. Using either of these techniques will keep the LCD screen's temperature below the experimentally derived maximum temperature of 75°C. Additionally, the simulation's heating rate matches the experimental behavior, although the simulation has a slightly increased cooling rate compared to the experiment. One potential downfall to the staggered illumination technique is that after an 80s cycle consisting of active curing, passive curing, and recoating, the LCD temperature remains higher than it does for the non-staggered illumination cases. Additionally, further work will investigate whether staggering the illumination periods has any effect on the total light exposure required for curing or the feature resolution of cured parts.

These results show that the combination of wire grid polarizers and an LCD screen can be feasibly subjected to the high intensities of light needed to cure the PCHS-silicone. The following section discusses the optical characterization of the light patterning system.

4. 2. Light Patterning Characterization

Transmittance experiments were conducted on film polarizers and wire grid polarizers at four UV and near-UV wavelengths to determine how the light transmittance decreases at shorter wavelengths. Light intensity was measured before and after each polarizer, and the percentage of light transmitted is shown in Table 1. The transmittance efficiency of light through a film polarizer is shown to decrease rapidly at shorter wavelengths, while the wire grid polarizer retains a higher percentage of light transmitted at every wavelength. This increase in performance between wire grid and film polarizers is most significant at wavelengths below 400 nm. The experimental transmittance results for 405 nm light match the expected values for film and wire grid polarizers of 25% and 44% within approximately 10% error [29] [30].

Table 1: Percent transmittance through film and wire grid polarizers

Wavelength (nm)	Film Polarizer	Wire Grid Polarizer
365	0.0	34.3
385	1.1	39.3
405	22.9	39.1
450	34.8	42.5

Further transmittance measurements were performed on LCD screens with their original film polarizers intact and then replaced with wire grid polarizers to study both transmittance efficiency and ability to pattern UV and near-UV light. During these high-intensity illumination experiments, the temperature of the polarizers was monitored with surface mount thermocouples. Light intensity measurements were taken with the LCD displaying first a fully white screen followed by a fully black screen. The ratio between transmitted intensities for the white and black screens determines the contrast ratio, which is an initial measurement for how well the LCD patterns the incoming light field, where a lower contrast ratio indicates a smaller range between transmitted intensities through black and white screens and therefore, worse performance. Table 2 displays these contrast ratio results for both 385 and 405 nm light. The values presented for the white and black screens are the percentages of light transmitted based on an incoming light intensity of 1500 mW/cm^2. This transmittance efficiency can be used to predict the initial light intensity required to provide the necessary intensity at the printing surface.

Table 2: Percent transmittance through LCDs with film and wire grid polarizers

% Transmittance	**385 nm**			**405 nm**		
	White	Black	Contrast	White	Black	Contrast
Film/LCD/Film	1.1	0.05	21.3	3.0	0.07	43.4
WGP/LCD/Film	1.9	0.23	8.0	3.9	0.38	10.3
WGP/LCD/WGP	3.3	0.50	6.5	4.7	0.76	6.2

The experimental results presented in Table 2 confirm the trends observed for light transmission through a single film or wire grid polarizer, and similar trends are observed for combinations of the two types of polarizers when used with an LCD screen. The wire grid polarizers transmit a higher portion of light than the film polarizers do, with this effect being more pronounced at lower wavelengths. For 385 nm light, the use of WGPs instead of film polarizers increases transmittance through the LCD from 1.1 to 3.3%.

In addition to transmittance efficiency, the other important quality of a light patterning device is the contrast ratio. This contrast ratio, or the ratio of transmitted light through a white screen relative to a black screen, decreases significantly when using wire grid polarizers instead of the screen's original film polarizers. At 385 nm, the contrast ratio decreases from 21.3:1 to 6.5:1. Potential reasons for this decrease in contrast as well as experimental measurements of the Modulation Transfer Function, which show the decrease in contrast relative to feature size of alternating black and white line pairs, can be found in Appendix C.

4. 3. Two-Dimensional Patterns Cured using LCD with Wire Grid Polarizers

Following the MTF tests, which optically predicted the minimum resolvable feature sizes using this light patterning technique, curing tests were conducted to validate the technique's minimum printable feature sizes. A series of lines with thicknesses varying from 2 to 10 pixels (76.5 μm/pixel) with 20-pixel gaps was patterned on the LCD screen and illuminated for 10s under 4 mW/cm^2 of 385 nm light (Figure 10a). A second pattern was designed to investigate the minimum resolvable hole that could be cured. Figure 10b shows holes ranging from 5 to 20 pixels that were patterned on the LCD and illuminated for 6s to cure a layer of PR48.

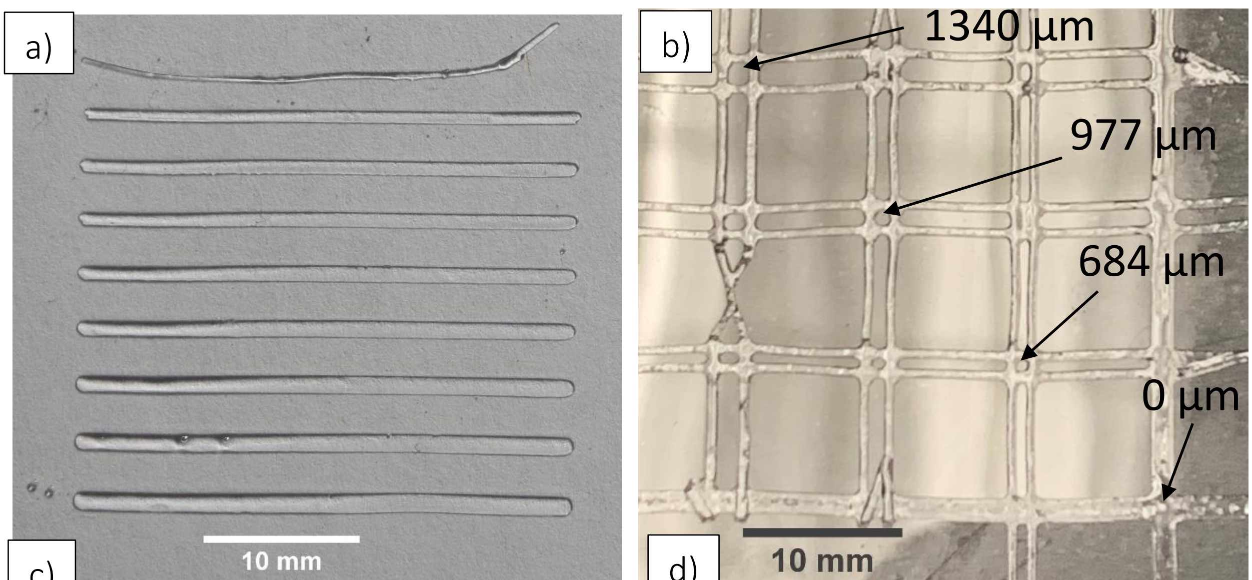

c)

Line Width	Projected (μm)	Printed (μm)
2 pixels	153	300
3 pixels	230	668
4 pixels	306	815
5 pixels	382	835

d)

Hole Width	Projected (μm)	Printed (μm)
5 pixels	383	0
10 pixels	765	684
15 pixels	1150	977
20 pixels	1530	1340

Figure 10: Lines and holes patterned on an a 13.3" 4K LCD with one film polarizer replaced with a wire grid polarizer; a, c) Two-to-ten-pixel lines printed out of PR48 with 500 ppm MEHQ with smallest resolved line of 300μm; b, d) Five-to-twenty-pixel holes printed out of PR48 with smallest resolved hole under 700 μm

Printed feature sizes are compared to patterned feature sizes for both lines and holes in Figure 10c and 10d, respectively. The printed lines are consistently overcured by approximately 100-200% due to the relatively long exposure of ten seconds, which was necessary in order for the 2-pixel line to resolve. Lower exposures of 6-8 seconds resulted in more accurately sized features, though lines patterned below 230 µm did not cure. The smallest resolvable holes in Figure 10b and 10d were the 10-pixel holes, which were overcured approximately 10% for a hole diameter of 680 µm instead of the patterned 765 µm. The other resolved holes, 15 and 20 pixels, were also overcured by 10-15%. The 5-pixel lines composing the grid in the “holes” test exhibited an average cured thickness of 520 µm, which is overcured from the patterned 382 µm, but less significantly than in the line curing test, which had an exposure of 10s as opposed to 6s for the holes test.

Using the same curing conditions as for the line test, a fractal tree with features ranging from 2 mm – 600 µm was cured with PR48 resin as shown in Figure 11. Features on the fractal tree were overcured similarly to the line test, as the smallest branches were patterned with three pixels, or 230 µm, but printed closer to 600 µm. The larger branches did not overcure as significantly; the tree trunk’s patterned thickness was 27 pixels (2.07 mm) versus its printed thickness of 2.08 mm.

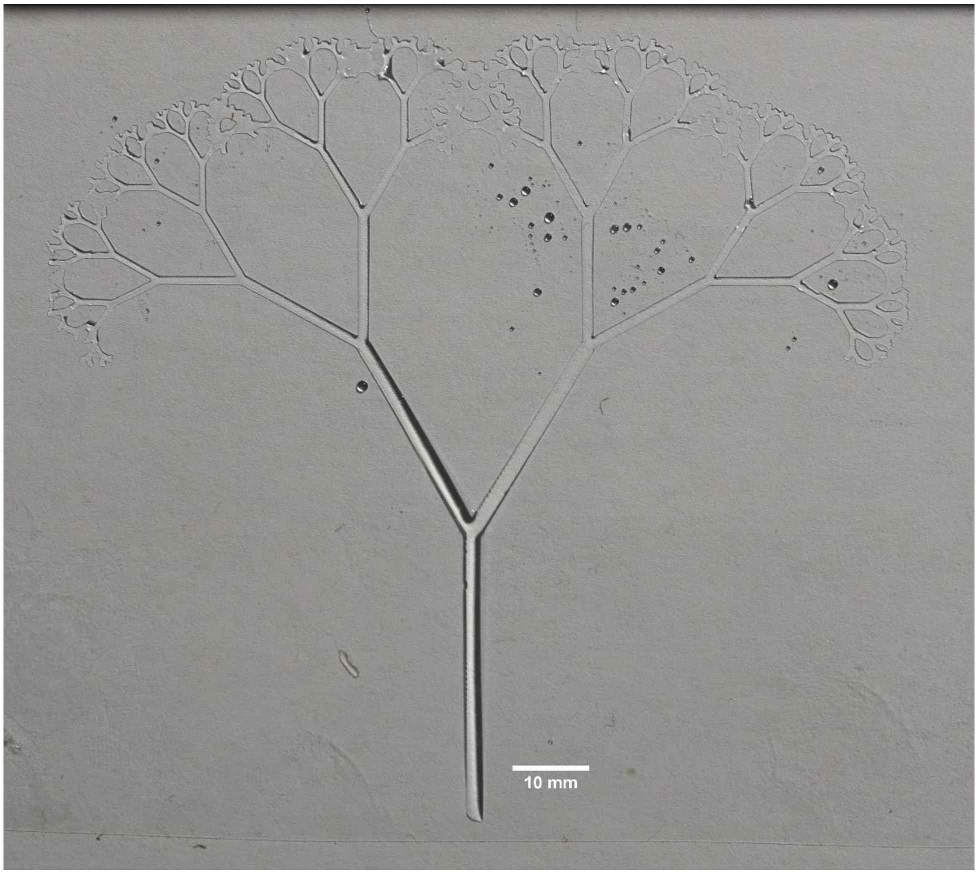

Figure 11: Fractal tree printed with smallest resolved features <600 μm

The prior test parts were all cured in PR48 to demonstrate the fine resolution control of the light patterning system; however, the use of wire grid polarizers is mainly necessary for resins that require much higher intensities and total flux to cure. PR48 was cured with an intensity at the build plane of 4 mW/cm^2 of 385 nm light for 6-10s. The PCHS-silicone, on the other hand, requires an intensity of at least 85 mW/cm^2 for 20s to initiate curing. A typical monochrome LCD screen cannot pattern this intensity of light without overheating in seconds, so the use of wire grid polarizers replacing the LCD's film polarizers is necessary to print with this resin.

With the use of wire grid polarizers, a UT and LLNL logo were printed using PCHS-silicone (See Figure 12). Both the UT and LLNL logos had overcured gaps between features, as the PCHS-silicone likely needs a higher concentration of photo-inhibitor than was used to resolve smaller gaps. The gap between the letters U and T was patterned with a 6.2 mm gap and resolved at 2.3 mm. Similarly, the gaps between each L were patterned to be 3.2 mm, and portions of the logo towards the base had overcured gaps of around 1.5 mm. However, the vertical gaps at the top of the logo were resolved at 3.4 mm, which is within 6% tolerance of the intended gap size. This difference in gap resolution could potentially be due to the resin tending to overcure where there is a higher density of transmitted light surrounding a feature, such as the center L, which is bounded by an additional L on either side. This phenomenon could explain why the gaps towards the top of the logo are not overcured, and this will be investigated further in future research.

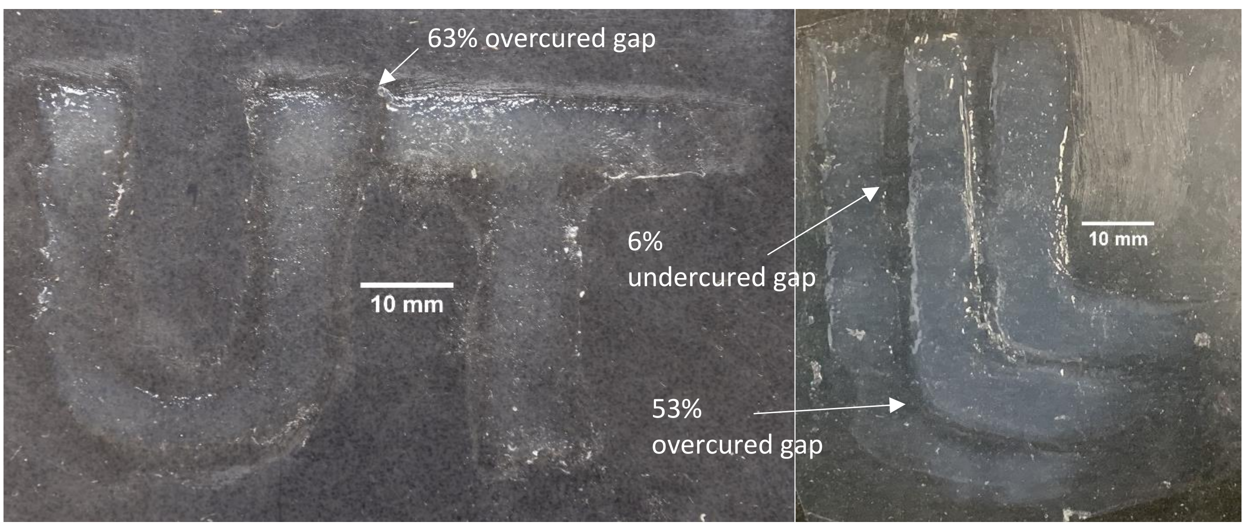

Figure 12: UT and LLNL logo printed out of Pt-catalyzed hydrosilylation reaction silicone

Although the logos printed in PCHS-silicone have printed resolutions an order of magnitude larger than features printed with PR48, this method of curing silicone using a UV-initiated, platinum-catalyzed hydrosilylation reaction has never been conducted on time scales relevant to 3D printing. This demonstration is an important first step in using stereolithography to additively manufacture silicones with mechanical properties and aging behavior similar to conventionally manufactured silicones.

5. Conclusions

This research proposes and validates a novel light patterning technique for stereolithography that involves replacing the film polarizers of a monochrome LCD screen with wire grid polarizers. The new approach to masked SLA solves some of the problems encountered with using materials that are less reactive to the relatively low light intensities and high wavelengths traditionally used in this printing process. The use of wire grid polarizers with an LCD screen allows the patterning of high-intensity, UV light over larger areas than any other digital light processing technique. Replacing the LCD's film polarizers with wire grid polarizers solves three challenges of using LCDs to pattern UV light: limited range of patterned wavelengths, low intensity of light, and low efficiency of transmission at all wavelengths of light. Wire grid polarizers are capable of polarizing light at both lower wavelengths and higher intensities than film polarizers with a higher transmission rate.

Wire grid polarizers are shown in this research to dynamically pattern light with wavelengths as low as 365 nm and with intensities exceeding 1700 mW/cm^2, while transmitting the UV light three times as efficiently as an LCD with its film polarizers. The maximum intensity of light patterned with this technique is limited by the thermal behavior of the LCD, as it can function only at temperatures below 75°C. Therefore, with increased cooling capabilities and shorter illumination durations, this technique could pattern light at even higher intensities than have been demonstrated here. Using the presented techniques of forced air convection with 5s illumination phases, the LCD with wire grid polarizers can pattern 1700 mW/cm^2 of 385 nm light for a total active curing time exceeding 20s without exceeding the LCD's maximum temperature. Future work is required to continue validating the effectiveness and longevity of this light patterning technique, including studying the thermal fatigue behavior of LCD screens as they are subjected to many cycles at heightened temperatures.

UV light is patterned over areas of up to 130 x 130 mm^2 with features of 230 µm at that size. However, these limitations are dependent only on the size and resolution of the liquid crystal device, and future work will explore tiling multiple wire grid polarizers to polarize a larger light field.

Additionally, as the light source for this research was an LED array and not a point source, the light could not be collimated; therefore, the optical path length of the light needed to be minimized after it was patterned by the LCD screen to avoid features blurring together. For this reason, the light patterning system in some portions of this research used a WGP as the first polarizer but retained one of the LCD's original film polarizers as the second. This arrangement allowed for a minimal optical path length after light passed through the liquid crystal so that smaller features could be patterned. This mixed polarizer technique still allows for high intensity printing, as the first polarizer is subjected to an order of magnitude higher light intensity than the second, allowing the wire grid polarizer to polarize the high initial intensities of light. Then, with only a small optical path length after the LCD, the film polarizer can pattern the light at significantly lower intensities. In future research, two wire grid polarizers could be used if the second WGP were patterned directly onto the distal surface of the LCD screen.

References

[1] C. Hull, "Apparatus for Production of Three-Dimensional Objects by Stereolithography". USA Patent US45753300A, 11 March 1986.

[2] 3D Systems, "Stereolithography Printers - Prototypes, tools and production parts with ProJet® and ProX® SLA 3D printers," 2019. [Online]. Available: https://www.3dsystems.com/sites/default/files/2019-12/3d-systems-SLA-brochure-usen-2019-11-15-web.pdf. [Accessed September 2019].

[3] A. Bertsch, S. Zissi, J. Y. Jezequel, S. Corbel and J. C. Andre, "Microstereophotolithography using a liquid crystal display as dynamic mask-generator," *Microsystem Technologies,* vol. 3, pp. 42-47, 1997.

[4] C. Chatwin, M. Farsari, S. Huang, M. Heywood, P. Birch, R. Young and J. Richardson, "UV microstereolithography system that uses spatial light modulator technology," *Applied Optics,* vol. 37, no. 32, pp. 7514-7522, 1998.

[5] S. Monneret, H. Le Gall, V. Badé, F. Devaux, A. Mosset and E. Lantz, "Dynamic UV microstereolithography," *The European Physical Journal - Applied Physics,* vol. 20, no. 3, pp. 213-218, 2002.

[6] A. Limaye and D. W. Rosen, "Quantifying dimensional accuracy of a mask projection micro stereolithography system," in *Proceedings of the Solid Freeform Fabrication Symposium*, Austin, TX, 2004.

[7] J. C. Choi, M. D. Irwin and R. B. Wicker, "DMD-based 3D micro-manufacturing," in *Proceedings Volume 7596, Emerging Digital Micromirror Device Based Systems and Applications II*, San Francisco, CA, 2010.

[8] C. Sun, N. Fang, D. M. Wu and X. Zhang, "Projection micro-stereolithography using digital micro-mirror dynamic mask," *Sensors and Actuators A: Physical,* vol. 121, no. 1, pp. 113-120, 2005.

[9] G. W. Hadipoespito, Y. Yang, H. Choi, G. Ning and X. Li, "Digital micromirror device based microstereolithography for micro structures of transparent photopolymer and nanocomposites," in *Proceedings of the Solid Freeform Fabrication Symposium*, Austin, TX, 2003.

[10] K. Takahashi and J. Setoyama, "A UV-exposure system using DMD," *Electronics and Communications in Japan (Part II Electronics),* vol. 83, no. 7, pp. 56-58, 2000.

[11] Texas Instruments, "High-accuracy 3D scanning using Texas Instruments DLP® technology for structured light," 2018. [Online]. Available: http://www.ti.com/lit/wp/dlpy005a/dlpy005a.pdf. [Accessed Jan 2019].

[12] X. Zheng, J. DeOtte, M. P. Alonso, G. R. Farquar, T. H. Weisgraber, S. Gemberling, H. Lee, N. Fang and C. M. Spadaccini, "Design and optimization of a light-emitting diode projection micro-stereolithography three-dimensional manufacturing system," *Review of Scientific Instruments,* vol. 83, no. 125001, 2012.

[13] Texas Instruments, "DLP9500UV DLP® 0.95 UV 1080p 2x LVDS Type A DMD datasheet (Rev. C)," March 2017. [Online]. Available: http://www.ti.com/lit/ds/symlink/dlp9500uv.pdf. [Accessed January 2019].

[14] B. D. Moran, "Large area projection micro stereolithography". USA Patent US20160303797A1, 16 April 2015.

[15] A. Bertsch, J. Y. Jezequel and J. C. Andre, "Study of the spatial resolution of a new 3D microfabrication process: the microstereophotolithography using a dynamic mask-generator technique," *Journal of Photochemistry and Photobiology A: Chemistry,* vol. 107, pp. 275-281, 1997.

[16] H.-C. Cheng, I. Ben-David and S.-T. Wu, "Five-primary-color LCDs," *Journal of Display Technology,* vol. 6, no. 1, pp. 3-7, 2010.

[17] G. Fei, T. Wei, Q. Shi, Y. Guo, H. Oprins and S. Yang, "Preliminary Study on Hybrid Manufacturing of the Electronic-Mechanical Integrated Systems (EMIS) via the LCD Stereolithography Technology," in *Solid Freeform Fabrication Symposium*, Austin, 2019.

[18] eSUN Industrial Co., "iSUN3D LCD3.0," 2007. [Online]. Available: http://www.esun3d.net/products/247.html. [Accessed June 2020].

[19] L. Huang, R. Jiang, J. Wu, J. Song, H. Bai, B. Li, Q. Zhao and T. Xie, "Ultrafast Digital Printing toward 4D Shape ChangingMaterials," *Advanced Materials,* vol. 29, no. 7, 2016.

[20] X. Wu, C. Xu and Z. Zhang, "Flexible film separation analysis of LCD based mask stereolithography," *Journal of Materials Processing Technology,* vol. 288, 2021.

[21] X. Wu, C. Xu and Z. Zhang, "Preparation and optimization of Si3N4 ceramic slurry for low-cost LCD mask stereolithography," *Ceramics International,* 2020.

[22] Z. Wang, N. Martin, D. Hini, B. Mills and K. Kim, "Rapid Fabrication of Multilayer Microfluidic Devices Using the Liquid Crystal Display-Based Stereolithography 3D Printing System," *3D Printing and Additive Manufacturing,* vol. 4, no. 3, pp. 156-164, 2017.

[23] H. Svajdlenkova, O. Sausa, G. Peer and C. Gorsche, "In situ investigation of the kinetics and microstructure during photopolymerization by positron annihilation technique and NIR-photorheology," *RSC Adv.,* vol. 8, pp. 37085-37091, 2018.

[24] S. C. Shit and P. Shah, "A Review on Silicone Rubber," *National Academy Science Letters,* vol. 36, pp. 355-365, 2013.

[25] N. A. Rodriguez, S. Ruelas, J.-B. Forien, N. Dudukovic, J. DeOtte, J. Rodriguez, B. Moran, J. P. Lewicki, E. B. Duoss and J. S. Oakdale, "3D Printing of High Viscosity Reinforced Silicone Elastomers," *Polymers,* vol. 13, no. 14, p. 2239, 2021.

[26] J. M. Lambert, "The nature of platinum in silicones for biomedical and healthcare use," *Journal of Biomedical Materials Research B: Applied Biomaterials,* vol. 78, pp. 167-180, 2006.

[27] J. Oxman and L. Boardman, "Radiation-activated hydrosilation reaction in the presence of platinum complexes". USA Patent WO9210543A1, 1992.

[28] K. Obata, S. Slobin, A. Schonewille, A. Hohnholz, C. Unger, J. Koch, O. Suttmann and L. Overmeyer, "UV laser direct writing of 2D/3D structures using photo-curable polydimethylsiloxane (PDMS)," *Applied Physics,* vol. 123, no. 7, p. 495, 2017.

[29] B. Whitehead and R. Oszust, "Economy Film Polarizers," 25 10 2018. [Online]. Available: https://www.thorlabs.com/newgrouppage9.cfm?objectgroup_id=7081. [Accessed June 2019].

[30] D. Daranciang and E. Poinescu, "Wire Grid Polarizers on Glass Substrates," 27 10 2014. [Online]. Available: https://www.thorlabs.com/newgrouppage9.cfm?objectgroup_id=5510. [Accessed June 2019].

[31] N. L. Koren, "Correcting Misleading Image Quality Measurements," in *IS&T International Symposium on Electronic Imaging*, San Francisco, CA, 2020.

[32] A. D. Raisanen, M. D. Presnar, Z. Ninkov, K. D. Fourspring, L. Meng and J. Kerekes, "Simulation of practical single-pixel wire-grid polarizers for superpixel stokes vector imaging arrays," *Optical Engineering,* vol. 51, no. 1, 2012.

[33] M. Polyanskiy, "Refractive Index Database - Glass - BK7 - N-BK7 (SCHOTT)," [Online]. Available: https://refractiveindex.info/?shelf=glass&book=BK7&page=SCHOTT. [Accessed May 2020].

[34] Filmetrics, "Refractive Index of ITO, Indium Tin Oxide, InSnO," [Online]. Available: https://www.filmetrics.com/refractive-index-database/ITO/Indium-Tin-Oxide-InSnO. [Accessed May 2020].

[35] S.-T. Wu, "Absorption measurements of liquid crystals in the ultraviolet, visible, and infrared," *Journal of Applied Physics,* vol. 84, no. 8, pp. 4462-4465, 1998.

[36] S. Huang, M. I. Heywood, R. C. D. Young, M. Farsari and C. R. Chatwin, "Systems control for a micro-stereolithography prototype," *Microprocessors and Microsystems,* vol. 22, no. 2, pp. 67-77, 1998.

[37] C. Chatwin, M. Farsari, S. Huang, M. Heywood, P. Birch, R. Young and J. Richardson, "UV microstereolithography system that uses spatial light modulator technology," *Applied Optics,* vol. 37, no. 32, pp. 7514-7522, 1998.

[38] C. Soutar and H. Lu, "Determination of the physical properties of an arbitrary twisted-nematic liquid crystal cell," *Optical Engineering,* vol. 33, no. 8, 1994.

[39] P. M. Lambert, E. A. Campaigne III and C. B. WIlliams, "Design Considerations for Mask Projection Microstereolithography Systems," in *Solid Freeform Fabrication Symposium*, Austin, TX, 2013.

Acknowledgements

This work was performed under the auspices of the U.S. Department of Energy by Lawrence Livermore National Laboratory under Contract DE-AC52-07NA27344 and reviewed for external release under IM Review #: LLNL-JRNL-831192.

The LED arrays used in this work were provided with financial support from Violumas (Fremont, CA).

Appendix A. DMD Power Transmission

Digital micromirror devices (DMDs) are widely used in DLP printers to rapidly cure photopolymers with high resolution; however, there are significant limitations to using a DMD to pattern high intensity UV light over large areas. Both LCDs and DMDs are limited in form factor and resolution, with the largest high resolution DMDs being 0.9" in size at 4K resolution with 7.6 µm pixels or 0.95" at 1080p with 10.8 µm pixels (see Figure 13a) [13]. Therefore, an image patterned on a DMD that is magnified to a 30" image would generate pixels between 250 and 350 µm in size. In comparison, a monochrome 10MP 30" LCD has a pixel size of 158 µm. In addition to the fixed ratio of pixel size to image projection size, the maximum light intensity output is another reason a DMD struggles to work for large area applications. Even the largest UV DMDs are limited to a maximum intensity of 11 W/cm^2 input into the chip for 400-420 nm light, or a total power of 26.6 W (see Figure 13b) [13]. For light ranging from 363 – 400 nm, the maximum input intensity is 2.5 W/cm^2 for a total intensity of 6 W.

a)

		VALUE	UNIT
Number of active micromirror columns (1)		1920	micromirrors
Number of active micromirror rows (1)		1080	micromirrors
Micromirror (pixel) pitch (1)		10.8	µm
Micromirror active array width (1)	M × P	20.736	mm
Micromirror active array height (1)	N × P	11.664	mm
Micromirror array border (1) (2)	Pond of micromirrors (POM)	10	micromirrors/side

b)

< 363 nm (8)	2	mW/cm^2
363 to 400 nm (9)	2.5	W/cm^2
	6	W
400 to 420 nm (9)	11	W/cm^2
	26.6	W

Figure 13: a) Physical characteristics of DLP9500; b) Illumination Power Density for DLP9500 (68% efficiency) [13]

When this patterned light field is constrained to a small area, high intensities are possible even with the DMD's 68% patterning efficiency. However, to project an image with its shortest axis at least 400 mm in length, which is the target achieved by the 30" LCD monitor, the DMD image would need to be magnified by a factor of 34.3 from the chip size. The maximum intensity of this magnified image would be 1.4 mW/cm^2. By using an LCD with a wire grid polarizer, which is patterning light on the same form factor as it is printing, the intensity of patterned 385 nm light at the printing surface can reach 80-100 mW/cm^2.

Appendix B. Modeling Polarizers

The polarization of a ray of light is defined in COMSOL using the polarization ellipse's semi-major and semi-minor axes in global cartesian coordinates. An elliptical polarization is a general state of polarization that defines the tip of the light's electric field as it travels along the direction of propagation. For linear polarizations, the electric field tip oscillates back and forth along a single axis that is orthogonal to propagation. Similarly, the electric field in circular polarizations traces out the path of a circle in the same transverse plane. Elliptical polarizations can define any combination of these two special states of polarization and are represented by the Jones vector, which consists of the x and y components of the 3D representation of each ray's electrical field, as seen in Equation 3.

$$\begin{pmatrix} E_{0x}e^{i\Phi_x} \\ E_{0y}e^{i\Phi_y} \end{pmatrix} \tag{3}$$

For example, the Jones vector for horizontal (x) or vertical (y) polarizations is (1, 0) or (0, 1), respectively. An additional representation of polarization is the Stokes vector (S_0, S_1, S_2, S_3) whose parameters are defined by Equation 4.

$$\begin{gathered} S_0 = I(0,0) + I\left({}^{\pi}/_{2}, 0\right) \\ S_1 = I(0,0) - I\left({}^{\pi}/_{2}, 0\right) \\ S_2 = I\left({}^{\pi}/_{4}, 0\right) - I\left({}^{3\pi}/_{4}, 0\right) \\ S_3 = I\left({}^{\pi}/_{4}, {}^{\pi}/_{2}\right) - I\left({}^{3\pi}/_{4}, {}^{\pi}/_{2}\right) \end{gathered} \tag{4}$$

These Stokes parameters can be physically described as the total intensity of x and y polarizations combined, the difference between x and y polarized light, the difference between light polarized 45° (diagonal) and -45° (anti-diagonal) from the y axis, and the difference between right-handed and left-handed circular polarizations.

COMSOL's Ray Optics module additionally represents the polarization ellipse through six variables: the global x, y, and z coordinates making up the endpoints of the ellipse's semi-major and semi-minor axes. Prior to using this polarization ellipse to define characteristics of the wire grid polarizer's behavior, we need to rotate the polarization ellipse from its global coordinates P_{ax}, P_{ay}, and P_{az} to the ray's local coordinate system, which only has components P_{ax}' and P_{ay}', which are the components defined by the Jones vector. This is accomplished using the Rodrigues' Rotation Formula,

$$V_{rot} = Vcos(\theta) + (K \times V)\sin(\theta) + K(K \cdot V) \tag{5}$$

where V is the vector consisting of (P_{ax}, P_{ay}, P_{az}), K is the unit vector $P_{az}\hat{k} \times \left(P_{ax}\hat{\imath} + P_{ay}\hat{\jmath}\right)$, and θ is defined as $\tan^{-1}\left(\frac{abs(P_{az})}{\sqrt{P_{ax}^2+P_{ay}^2}}\right)$.

This rotation is validated by observing the z component of each ray's polarization ellipse's semi-major axis, which should be zero, as no component of the ellipse lies in the direction of propagation. A plot of these components is shown in Figure 14.

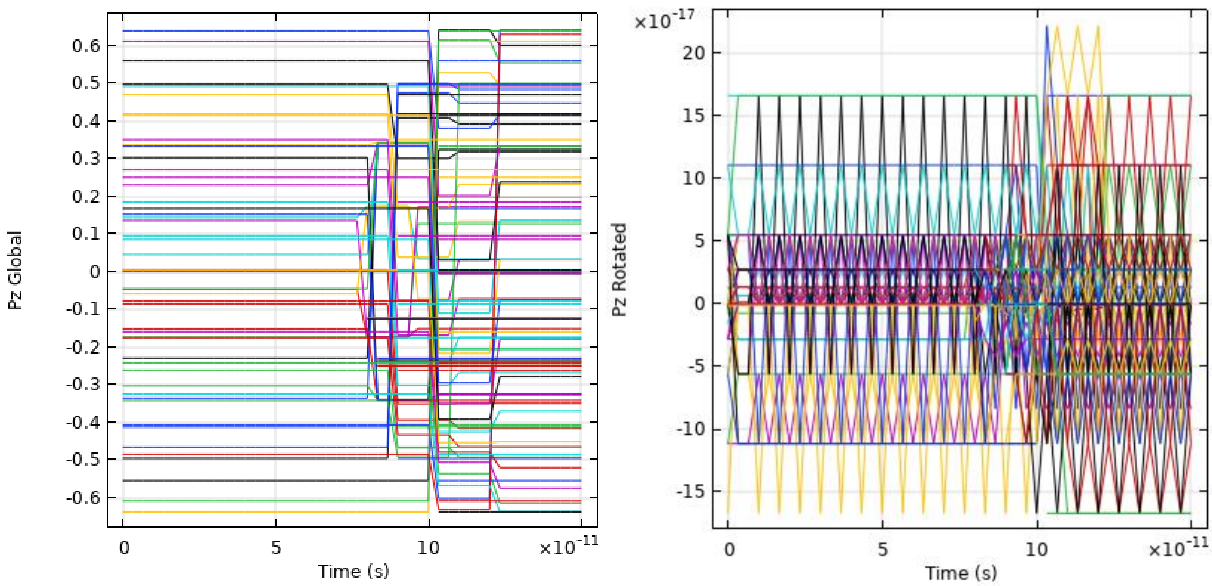

Figure 14: Z component of polarization ellipse's semi-major axis before and after rotating to ray's local coordinates

To simulate a wire grid polarizer, two main responses of the polarizer to a light ray need to be modeled. First, the polarizer should reflect and transmit portions of each ray's intensity as a function of the ray's polarization compared to the polarizer's transmission axis. Second, the polarizer should rotate each ray's polarization ellipse about the direction of propagation so that the transmitted ray has a polarization that is aligned with the transmission axis and the reflected ray has a polarization orthogonal to the transmission axis.

To start, the polarizer's domain is given a diffraction grating boundary condition that inherently transmits refracted rays and creates new reflected rays. This contrasts with the linear polarizer boundary condition, which can only transmit rays and has no ability to generate new reflected rays. Wire grid polarizers have previously been modeled as zero order diffraction gratings; however, in this simulation the diffraction grating condition is used only as the framework through which a wire grid polarizer can be modeled [32]. Since both reflectance and transmittance for this diffraction grating boundary condition can be defined as functions of user created variables, variables P_{ax}' and P_{ay}' were created to express the rotated components of a ray's polarization ellipse as defined by Equation 5. The ratio of these x' and y' polarization components for each ray can then be used in conjunction with both an experimentally derived transmittance or reflectance efficiency constant (T_p or T_r) as well as the unit vector of the polarizer's transmission axis (T_{px} and T_{py}) to define transmittance and reflectance as follows:

$$T=T_p\frac{\left(P_{ax}'\hat{\imath}+P_{ay}'\hat{\jmath}\right)\cdot\left(T_{px}\hat{\imath}+T_{py}\hat{\jmath}\right)}{\left|P_{ax}'+P_{ay}'\right|}$$
$$R=T_r\frac{\left(P_{ax}'\hat{\imath}+P_{ay}'\hat{\jmath}\right)\cdot\left(1-T_{px}\hat{\imath}+1-T_{py}\hat{\jmath}\right)}{\left|P_{ax}'+P_{ay}'\right|} \qquad (6)$$

These definitions use the dot product of the polarization ellipse semi-major axis and the polarizer's transmission axis to find the relative proportion of the ellipse that is aligned with the transmission axis. The same technique is used later in this discussion to define the angle at which the polarization ellipse must be rotated.

T_p and T_r for 385 nm light are 0.38 and 0.45, respectively, and are determined from spectroscopy results. The simulation's modeling of transmittance and reflectance is validated by setting T_p and T_r each equal to 0.5 and creating an incoming ray with a diagonal polarization. The resultant intensity for both reflected and transmitted rays is observed to be half of the incoming intensity, and these measurements are shown in Figure 15.

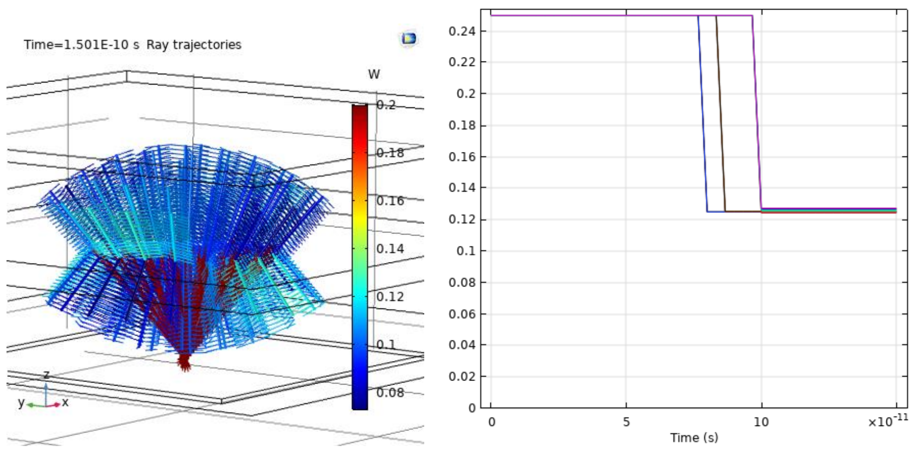

Figure 15: Reflected and transmitted rays each with half their starting power from the point source

COMSOL's equation editor enabled the modification of the normalized Stokes parameters for both rotated-refracted and rotated-reflected rays. These normalized Stokes parameters, S_{n1}, S_{n2}, and S_{n3}, are equivalent to S_1, S_2, and S_3 normalized by the total intensity, S_0. Since this simulation only deals with linearly polarized light, whether vertical, diagonal, or skewed, only S_{n1} and S_{n2} are applicable for modeling the polarizer's behavior. These two normalized Stokes parameters represent the difference between vertical and horizontal polarizations as well as diagonal and anti-diagonal polarizations, and they can be modified to model the second function of the polarizer: rotating each ray's polarization ellipse to be aligned with the polarizer's transmission axis.

For this simulation, since the transmission axis of the polarizer is aligned with the global y axis, the angle between this transmission axis and the polarization ellipse's semi-major axis for each incoming ray can be determined through the inverse tangent of P_{ax}' and P_{ay}', the same locally defined polarization components previously used to define reflectance and transmittance. This angle is the angle which each transmitted ray's polarization ellipse must be rotated about to be aligned with the transmission axis. This rotation is accomplished through modifying the normalized Stokes parameters as seen in Equation 7.

$$\begin{bmatrix} S_{n1}' \\ S_{n2}' \end{bmatrix} = \begin{bmatrix} \cos 2\theta & -\sin 2\theta \\ \sin 2\theta & \cos 2\theta \end{bmatrix} \begin{bmatrix} S_{n1} \\ S_{n2} \end{bmatrix} \tag{7}$$

Due to the possibility that the angle between the polarization ellipse's semi-major axis for an incoming ray and the transmission axis could be represented offset by 180°, a pre-processing step before the rotation was applied. The normalized Stokes parameters S_{n1} and S_{n2} for each reflected and transmitted ray were re-initialized to be (1,0) and (0,1), respectively, before determining and applying the rotation to align the polarization ellipse with the transmission axis. This ensured a consistent calculation of θ between the semi-major axis and transmission axis for each ray. Following this, the polarization ellipse was rotated by any residual angle between P_{ax}' and P_{ay}' and the transmission axis as shown in Equation 7 to account for the rare cases in which the re-initialized Stokes parameters did not correctly reorient the ray's polarization to be aligned with the transmission axis. This function of the new polarizing boundary condition is verified in Figure 16a, which shows rays being traced from a point source that are transmitted through the polarizer. The rays are diagonally polarized to start, so they lose half their intensity to reflections and, after passing through the polarizer, all have polarizations aligned with the transmission axis, which in this simulation was defined as the y axis. Figure 16b plots the y component of the polarization ellipse, P_{ay}'. Both the x and y polarizations began as diagonal orientations with values of $\pm\sqrt{2}/2$, and after passing through the polarizer, x polarizations changed to zero and the plotted y polarizations changed to ±1.

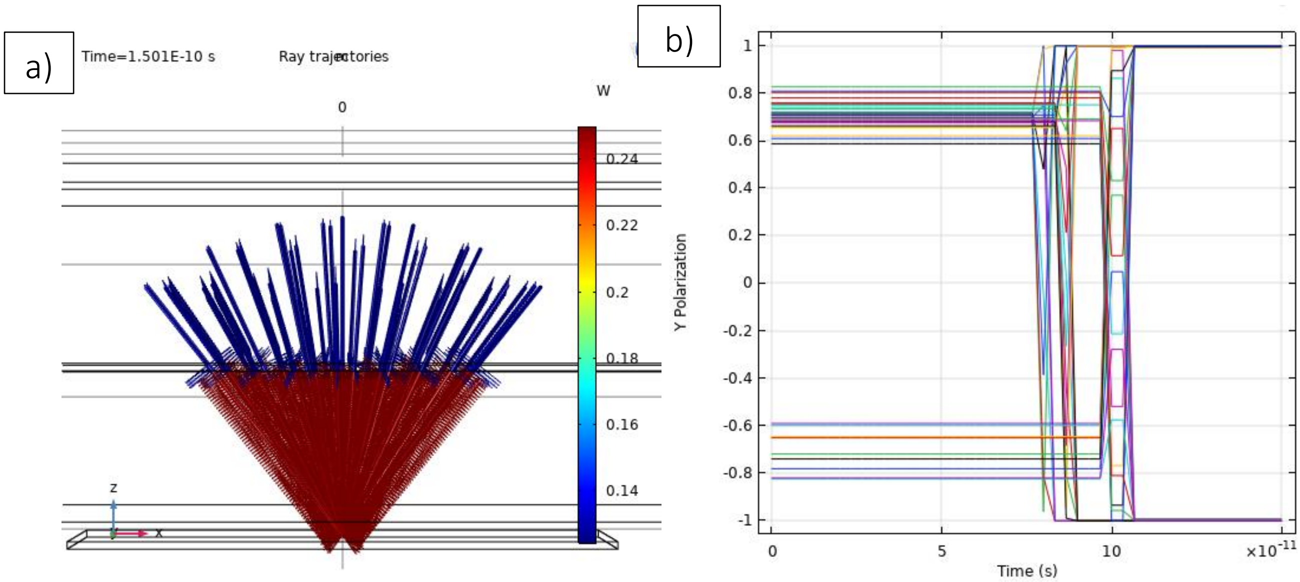

Figure 16: a) Rays are transmitting half their starting power and their polarization ellipse semi-major axes have been rotated to be aligned with the transmission axis (y), b) Y component of each ray's polarization ellipse goes from diagonal to ±1

Appendix C. Contrast and Modulation Transfer Function

From experimental results, replacing an LCD's film polarizers with wire grid polarizers significantly increases light transmission, but also decreases the contrast of the system. This decrease in contrast could be related to the increased optical path length, or the distance the light travels between the LCD, which rotates the polarization of the light, to the second polarizer, which patterns the light. When diffuse light travels a longer distance, a greater portion of light from each LCD pixel bleeds into surrounding pixels, making it more difficult for the LCD to pattern light. As the wires on the wire grid polarizer are mounted on a glass substrate, the light must travel through the substrate prior to being patterned. This creates a longer path length than occurs when using a film polarizer. Further research will be conducted to explore the relationship between the air gap and the contrast. Additionally, film polarizers are applied in a factory with high levels of precision in terms of orienting the polarizer and LCD planes parallel to one another as well as orienting the transmission axes of the two polarizers perpendicular to one other. Although the wire grid polarizers decrease achievable contrast, their use, at least as the first polarizer that must withstand the greatest intensity of light, is necessary to prevent the LCD from overheating when patterning high-intensity UV light.

MTF measurements show the decrease in contrast as progressively smaller features are patterned by the LCD screen. Line pairs with increasing spatial frequencies were patterned by the LCD screen and imaged by a camera with a 25 mm focal length lens. The MTF for each set of line pairs was calculated from the difference in their measured black and white intensities. An example image and intensity reading for patterned 385 nm light is shown in Figure 17. This image includes line pairs that are 2 pixels or 153 µm wide, for which the MTF is 0.42.

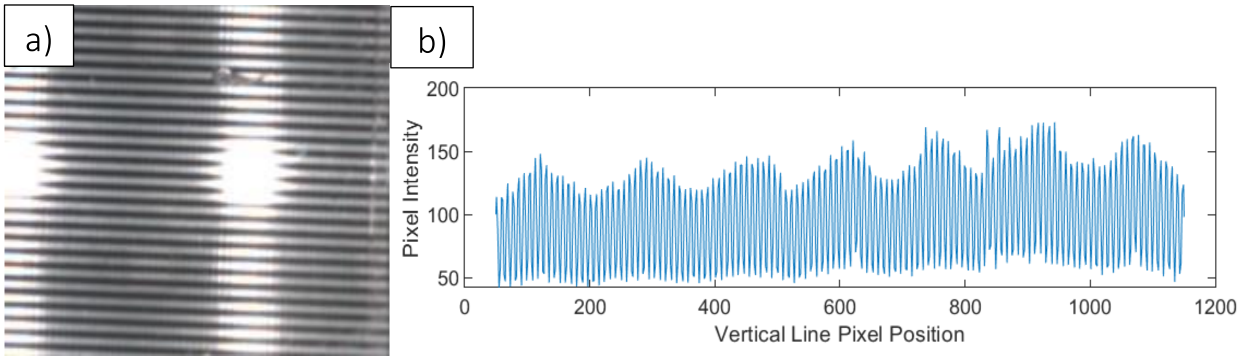

Figure 17: a) Image of line pairs patterned at 2 pixels/line. b) Intensity readings taken along a vertical line orthogonal to the patterned line pairs

In Figure 17a, visible bright spots can be seen which correspond to the placement of the LEDs in the array. However, these bright spots are solely an artifact of the camera's imaging technology. Due to the relatively large depth of field of the lens compared to the focal plane's distance from the LED array, the CCD is receiving light gathered by the lens at a distance of 10 to 20 mm below and above the focal plane, resulting in the visible hotspots correlated to the placement of the LEDs. The light field was validated to be homogeneous at the focal plane by removing the 25mm lens and placing the CCD at the focal plane. Intensity measurements were constant at 700 ± 50 mW/cm^2 over the entire light field, so the hot spots were determined to be solely an artifact of the lens gathering light from outside of the focal plane and were ignored in processing intensity data for MTF calculations.

Line pairs ranging from one to five pixels/line, or 76.5 – 382.5 µm/line, were successively patterned and imaged to determine the minimum feature size resolvable by this light patterning system. For this research, an MTF of 0.5 was used to predict the expected minimum resolvable feature size. MTF is plotted against line size in Figure 18 below.

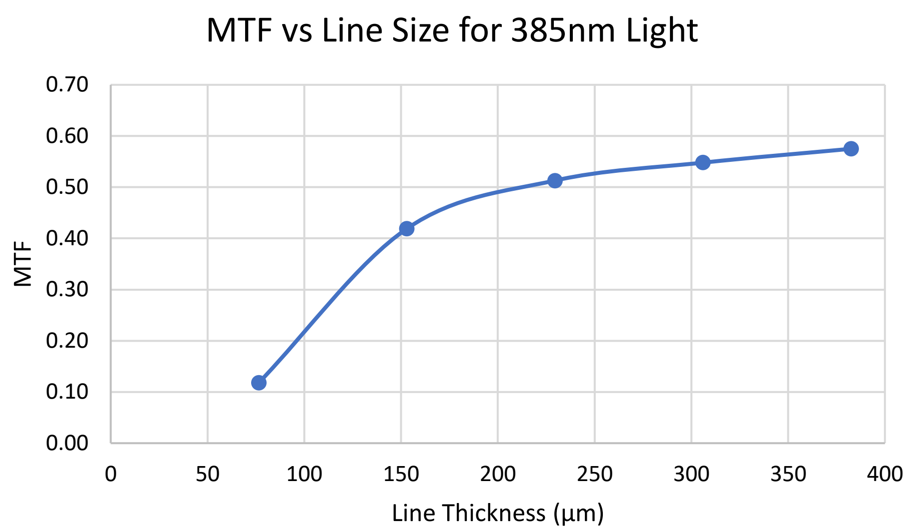

Figure 18: MTF measurements for patterned line pairs of varying spatial frequencies at 365nm light

At spatial frequencies of 1, 2, and 3 pixels per line, which correspond to 76.5, 153, and 229.5 µm thick lines, the MTF was 0.12, 0.42, and 0.51, respectively. These results reveal that for an LCD with 76.5 µm pixels, the wire grid polarizer and LCD light patterning system can pattern line pairs as small as three pixels or 230 µm using 385 nm light.